THE JOURNAL OF PHYSICAL CHEMISTRY C

Article

Cite This: J. Phys. Chem. C 2018, 122, 15078−15089

pubs.acs.org/JPCC

# Processing Methods for Obtaining a Face-On Crystalline Domain Orientation in Conjugated Polymer-Based Photovoltaics

Taylor J. Aubry,[†,∥] Amy S. Ferreira,[†,∥] Patrick Y. Yee,[†] Jordan C. Aguirre,[†] Steven A. Hawks,[‡] Matthew T. Fontana,[†] Benjamin J. Schwartz,*[,†,§] and Sarah H. Tolbert*[,†,‡,§]

[†]Department of Chemistry and Biochemistry, [‡]Department of Materials Science and Engineering, and [§]California NanoSystems Institute, University of California, Los Angeles, Los Angeles, California 90095-1569, United States

Supporting Information

**ABSTRACT:** The polymer chain orientation and degree of crystallinity within a polymer:fullerene bulk heterojunction (BHJ) photovoltaic can greatly impact device performance. In general, a face-on chain orientation is preferred for charge conduction through sandwich-structure photovoltaic devices, but for many conjugated polymers, an edge-on conformation is energetically favored. In this work, we examine the effects of different processing techniques on photovoltaics based on the poly[4,8-bis(2-ethylhexyloxy)-benzol[1,2-b:4,5-b′]dithiophene-2,6-diyl-*alt*-4-(2-ethylhexyloxy-1-one)thieno [3,4-*b*]thiophene-2,6-diyl] (PBDTTT-C):[6,6]-phenyl-$C_{71}$-butyric-acid-methylester ($PC_{71}BM$) materials combination. We examine the extent of polymer crystallinity and crystalline domain orientation using both traditional blend-casting (BC), where the polymer and fullerene are cast from a single, codissolved solution, as well as sequential processing (SqP), where the polymer film is deposited first, and then the fullerene is infiltrated into the polymer film in a second solution processing step. We show using two-dimensional grazing-incidence wide-angle X-ray scattering (GIWAXS) that BC leads to a disordered, isotropic polymer network in the resulting BHJ film with a correspondingly poor device efficiency. By contrast, SqP preserves the preferred face-on chain orientation seen in pure polymer films, yielding higher short-circuit currents that are consistent with the increased hole mobility of face-on oriented polymer chains. We also study the effects of the widely used processing additive 1,8-diiodooctane (DIO) on polymer chain orientation and crystallinity in photovoltaic devices made by both processing techniques. We show that DIO results in increased polymer crystallinity, and in devices made by BC, DIO also causes a partial recovery of the face-on PBDTTT-C domain orientation, improving device performance. The face-on chain orientation in SqP devices produces efficiencies similar to those of optimized BC devices made with DIO but without the need for solvent additives or other postprocessing steps.

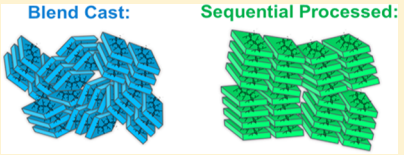


## INTRODUCTION

Organic photovoltaics (OPVs) are of interest due to their potentially low cost, ease of processing, and composition containing only earth-abundant elements. These devices typically consist of a semiconducting polymer as the primary photoabsorber and electron donor, paired with a fullerene derivative as the electron acceptor. Although reasonably high power conversion efficiencies (PCEs) can be obtained,[1−3] the overall device performance is highly sensitive to the morphology of the blended system.[4] To obtain optimal performance, the polymer and fullerene must have separated domains to enable efficient charge collection[5,6] but also must be mixed on length scales of less than ∼20 nm to prevent exciton recombination prior to charge separation.[7] The primary way this morphology is achieved is through blend-casting (BC), in which the polymer and fullerene are codissolved in solution and spun onto a conductive substrate.[8] In BC, the polymer and fullerene must partially demix during film formation to form a bicontinuous interpenetrating network, a process that is often assisted by the use of solvent additives[9−12] or via post-treatment steps involving solvent[13,14] or thermal annealing.[15−17] A more recently introduced method for forming polymer:fullerene BHJs is sequential processing (SqP).[18−26] In SqP, the polymer film is cast first, and then, the fullerene is infiltrated into the polymer in a second casting step using a quasi-orthogonal solvent or cosolvent blend chosen to swell but not dissolve the polymer underlayer, allowing mass action to drive fullerenes into the amorphous regions of the swollen polymer film.[22,27−32] The fullerene-casting solvent can be rationally selected on the basis of its Flory−Huggins $\chi$ parameter, which can be determined via a few simple ellipsometry measurements on solvent-swollen films, thereby avoiding the need for significant trial and error.[33] If necessary, fullerene intercalation in SqP also can be facilitated with a thermal annealing step.[8,29,34−36]

It is well-established that the polymer crystallinity in the active layers of BHJ photovoltaics is one of the key factors in determining carrier mobility and carrier extraction in polymer solar cells.[25,26] In addition to the total polymer crystallinity, however, the polymer domain orientation (i.e., "texture") also plays a major role in hole extraction from the device, which in turn influences both the short-circuit current and fill factor.[37,38]

**Received:** March 25, 2018
**Revised:** June 4, 2018
**Published:** June 11, 2018







DOI: 10.1021/acs.jpcc.8b02859
J. Phys. Chem. C 2018, 122, 15078−15089

Because of surface energetics, most semiconducting polymers prefer to lie with their side chains perpendicular to the surface (edge-on orientation of the backbone), requiring holes to hop between polymer chains to be extracted from the top and bottom contact electrodes in sandwich-structure devices.[39−41] Higher mobilities are found for carrier motion either along the polymer backbone or through a $\pi$-stacked network of polymer chains. Although it would be ideal to exploit the largest possible hole mobility, which is along the length of a semiconducting polymer chain, this would require a remarkably uncommon end-on polymer chain conformation in an OPV device.[42−47] Therefore, the best readily achievable mobility has the holes traveling through a stacked $\pi$-conjugation network, which is achieved for OPVs when all of the polymer chains orient face-on with respect to the substrate.[48]

For this reason, there has been much recent interest in determining whether the conjugated polymers used in OPV devices lie either face-on or edge-on with respect to the substrate. Indeed, when conjugated polymers have a face-on orientation in working devices, both hole mobility and extraction are improved.[37,38,49−54] One semiconducting polymer that is known to lie face-on when cast into pure films is poly[4,8-bis(2-ethylhexyloxy)-benzol[1,2-b:4,5-b′]dithiophene-2,6-diyl-*alt*-4-(2-ethylhexyloxy-1-one)thieno[3,4-*b*]-thiophene-2,6-diyl] (PBDTTT-C), which has been used extensively with blend-cast processing to make reasonably high-performing OPV devices.[55−62] Although the performance of blend-cast PBDTTT-C devices has been well-optimized,[55−62] the polymer crystallinity and domain orientation in BHJ devices has not been studied in depth.

In this paper, we present a detailed study of the crystallinity and orientation of PBDTTT-C polymer chains in both pure films and in BHJs produced by BC and SqP where the polymer is combined with [6,6]-phenyl-$C_{71}$-butyric-acid-methylester ($PC_{71}BM$). We also examine the effects of the widely used processing additive 1,8-diiodooctane[11,12,58−72] (DIO) in pure and BHJ films, as optimal blend-cast BHJs fabricated with PBDTTT-C require DIO.[58−62] We employ two-dimensional grazing-incidence wide-angle X-ray scattering (GIWAXS) to understand the extent to which the polymer maintains its face-on orientation in BHJ devices created using these different processing methods. We find that blend-casting leads to a more isotropic orientation of the PBDTTT-C crystalline domains in BHJ active layers but that the use of DIO improves device performance by both partially recovering the naturally preferred face-on orientation and improving overall polymer crystallinity. With SqP, we find that we are better able to preserve PBDTTT-C's intrinsic face-on orientation in BHJ active layers. This is because SqP works by swelling the amorphous regions of a polymer film with the fullerene-casting solvent, leaving the polymer crystalline domains relatively intact.[23,29] With the more favorable face-on orientation of PBDTTT-C in devices fabricated via SqP, we are able to match the device efficiencies of optimized blend-cast devices without the need for solvent additives such as DIO. The increased orientation control achieved with SqP and described in this work provides a further tool for researchers aiming to control multiple aspects of semiconducting polymer structure and domain orientation within functioning devices.

## EXPERIMENTAL SECTION

**Film Fabrication.** For GIWAXS and device studies, commercially available PBDTTT-C either was used as received or was combined with commercially purchased $PC_{71}BM$ via blend-casting or sequential processing. All PBDTTT-C solutions (pure and blended) were made at a polymer concentration of 10 mg/mL in *o*-dichlorobenzene, and all films were deposited by spin-coating. For blend-cast BHJ active layers, the solutions were made with a 1:1.5 wt/wt PBDTTT-C:$PC_{71}BM$ ratio, which when deposited yielded an active layer thickness of ∼90 nm. Sequentially processed active layers were fabricated by first spin-coating pure PBDTTT-C and then subsequently depositing the fullerene from a 10 mg/mL solution of $PC_{71}BM$ in a 1:1 v/v blend of 2-chlorophenol:dichloromethane (2CP:DCM) (chosen for optimal swelling of the polymer underlayer[33]), such that the final active layer thickness was also ∼90 nm. Some BHJs made by SqP used a 5 mg/mL $PC_{71}BM$ concentration in order to more clearly see the texture of the polymer diffraction peaks in GIWAXS experiments. Where noted, 3% v/v 1,8-diiodooctane (DIO) additive was added to either the blend-cast solution or the pure polymer solution samples. Also where noted, a methanol wash was performed to remove DIO from the films.[68−72] Films made for GIWAXS studies were cast onto silicon substrates (with a 1.8 nm $SiO_2$ native oxide layer) that were coated with a poly(ethylenedioxythiophene):poly(styrenesulfonic acid) (PEDOT:PSS) layer to replicate the bottom device interface; Si was chosen to minimize substrate diffraction. Active layer films for devices were fabricated from the same solutions as for the GIWAXS studies, and electrodes were evaporated to produce the final device structure: ITO/PEDOT:PSS/PBDTTT-C:$PC_{71}BM$/Ca/Al. Diodes for space-charge-limited current (SCLC) measurements were fabricated in the same way as the BHJ devices but using an architecture of ITO/PEDOT:PSS/active layer/Au to ensure majority hole carriers. All film thicknesses were measured using a Dektak 150 stylus profilometer. Further fabrication details can be found in the Supporting Information (SI).

**GIWAXS Measurements.** The two-dimensional GIWAXS measurements were performed at the Stanford Synchrotron Radiation Lightsource (SSRL) on beamline 11-3 using a wavelength of 0.9742 Å. Diffraction patterns were collected on a two-dimensional image plate with a sample to detector distance of 400 mm and a spot size of roughly 150 $\mu$m. A helium chamber was utilized to increase the signal-to-noise ratio. For the analysis of the GIWAXS data, the two-dimensional diffraction for each sample was integrated using WxDiff. The limits of the integration were changed on the basis of the orientation information desired. To obtain a full integration of a diffractogram, the integration limits over chi were from 0 to 180°. For in-plane, out-of-plane, and 45° integrations, the limits were 0−10°, 80−90°, and 40−50°, respectively. The intensities on the opposite sides of the diffractogram (90−180°) were also checked to ensure they were the same as the chosen limits. Each integration was background corrected for the substrate scattering. The subtractions were performed on the raw scattering data to ensure that no errors occurred due to background subtraction. To ensure reproducibility in diffraction intensity and shape, all samples were made and measured in triplicate, and if all three samples did not agree, samples were refabricated and rerun.



DOI: 10.1021/acs.jpcc.8b02859
J. Phys. Chem. C 2018, 122, 15078−15089

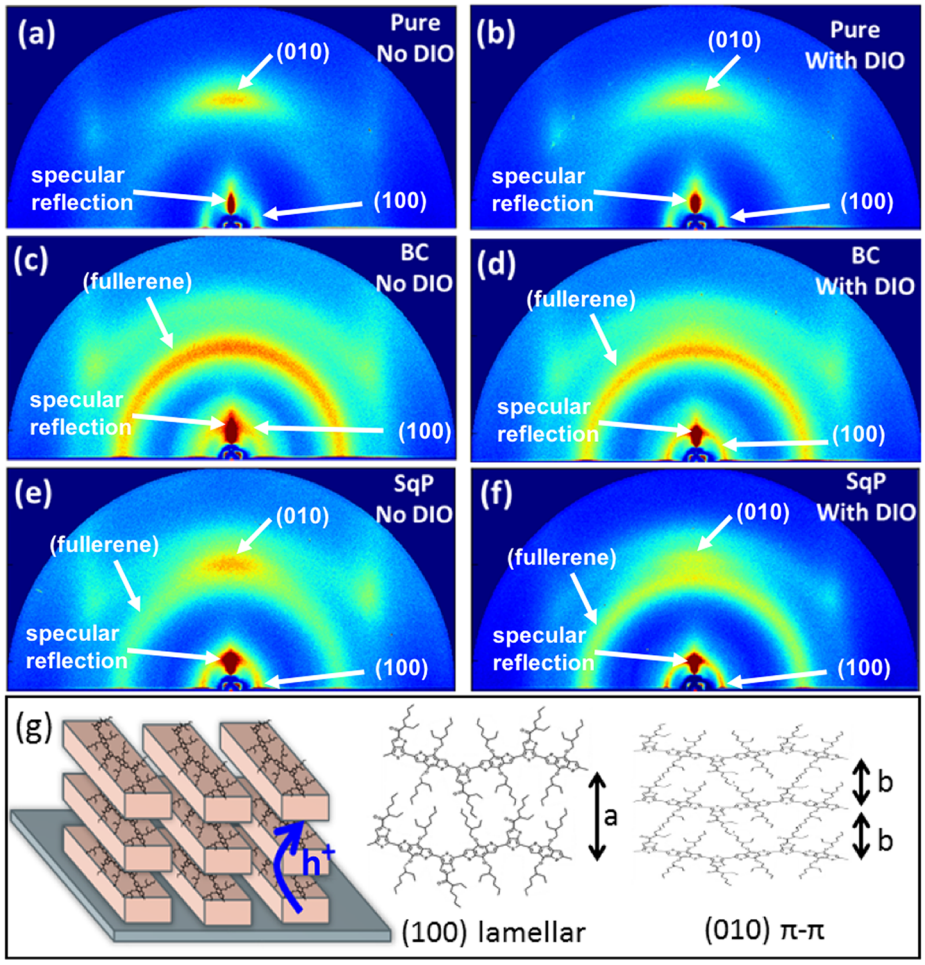


**Figure 1.** Raw GIWAXS diffractograms for pure polymer (a) and pure polymer with DIO (b) showing a face-on polymer orientation. Diffractograms for blend-cast (c,d) and sequentially processed (e,f) BHJs, both with (d,f) and without DIO (c,e) exhibit isotropic fullerene diffraction, but very different polymer chain orientations. Face-on polymer orientation is clearly seen in SqP films, while blend-cast films show more isotropic diffraction. A cartoon of face-on oriented polymer chains as well as cartoons depicting the (100)- and (010)-stacking directions are shown in (g).

**Device Measurements.** Photoluminescence spectra were collected on a Spex Fluorolog 3 spectrofluorometer using a 630 nm excitation wavelength, 5 s integration time, and 5 nm excitation and emission slit widths for all samples. Photovoltaic performance was measured in an argon atmosphere using a Keithley 2400 sourcemeter and AM-1.5 filtered light from a xenon arc lamp source equipped with a liquid light guide (Oriel). The incident light intensity on tested samples was adjusted to be 100 mW/cm$^2$ using a calibrated Si diode. SCLC measurements were taken on the same setup but without the light source. The dark $J-V$ curves were corrected for series resistance and fit to the Murgatroyd equation[73−75] to extract the steady-state mobilities (details of the fits can be found in the SI). EQE measurements were collected using a chopped (23 Hz) monochromatic beam (Newport TLS-300X) measured across a 50 Ω resistor using a SR830 lock-in amplifier. Because the currents are low, the voltage across the resistor and therefore the device is also low, which means that short-circuit conditions are well-maintained at all times. Multiple long-wave-pass filters (90% transmission cut-on at 345, 605, 850, 1030, and 1550 nm) were used during the measurement to remove high-energy light transmitted through the monochromator due to lower-order reflections. Each data point was taken from the amplitude readout of the lock-in and averaged for ∼5 time constants.

## RESULTS AND DISCUSSION

**I. Orientation of PBDTTT-C Crystallites Measured by 2-D GIWAXS.** Two-dimensional GIWAXS is a powerful tool that allows us to determine both the relative polymer crystallinity and the orientation of the crystalline domains. From the two-dimensional scattering patterns, the extent of polymer orientation can be determined by comparing the intensities of the (100) lamellar-stacking and (010) $\pi-\pi$-stacking peaks in both the conventional out-of-plane and in-plane scattering directions. The out-of-plane scattering reports only on those diffraction planes oriented parallel to the plane of the substrate, while in-plane scattering focuses on diffraction planes oriented perpendicular to the plane of the substrate. To study how the polymer structure changes with different processing conditions, we measured the two-dimensional X-ray scattering from both blend-cast and sequentially processed PBDTTT-C:$PC_{71}BM$ BHJ active layers in addition to pure PBDTTT-C films with and without DIO, as shown in Figures 1a−f.

*A. Face-On Structure of Pure PBDTTT-C Films.* From the raw diffractogram of the pure polymer (Figure 1a), the



DOI: 10.1021/acs.jpcc.8b02859
J. Phys. Chem. C 2018, 122, 15078−15089

preference for face-on orientation of the polymer domains can clearly be seen: the (100) lamellar peak is located primarily in-plane, and the (010) $\pi-\pi$-stacking peak is seen primarily in the out-of-plane direction, in agreement with the literature.[61] A cartoon depicting this face-on orientation of the PBDTTT-C polymer chains in the pure polymer film is shown in Figure 1g.

The addition of the solvent additive DIO to blend-cast solutions of polymers and fullerenes has been shown to improve the power conversion efficiency in a variety of systems[68−72] and in particular has been effective for improving devices made with PBDTTT-C.[58−62] Thus, we also looked at the effects of DIO on the structure of pure PBDTTT-C and sequentially processed BHJ films in addition to the well-studied blend-cast system with $PC_{71}BM$.[55−62] We find that adding DIO to solutions when casting pure polymer films does not change the polymer domain orientation (Figure 1b). For blend-cast and sequentially processed BHJ films, however, isotropic scattering from the fullerene is observed near the polymer (010) peak, making it difficult to see the polymer (010) diffraction peak in some cases. Even though the raw data cannot be used to determine polymer chain orientation in all cases, clear (010) scattering can still be seen in the out-of-plane direction for the sequentially processed films, suggesting that this method preserves the face-on orientation of the pure polymer. For a more detailed analysis of the chain orientation across processing conditions, selective integrations of the data are needed, as presented below.

For pure PBDTTT-C films, we radially integrated the two-dimensional diffractograms shown in Figure 1 to obtain information on the crystallinity and crystallite size, as depicted in Figure 2a. The fitted peak areas and coherence lengths, which give quantitative information about the overall crystallinity and crystallite size, are given in Table S1 of the SI. The pure polymer exhibits characteristic (100) and (010) scattering peaks at 0.33 and 1.57 $Å^{-1}$, respectively. Upon the addition of DIO, a marked increase of over 50% in the overall crystallinity of the pure polymer is observed. It is well-established that, due to its low volatility, DIO tends to remain in polymer films, where it can be detrimental to device performance if it is not properly removed.[70−72] Furthermore, it has been shown that the addition of DIO increases time for crystallite formation in BHJs.[76] Thus, the low volatility of DIO compared to the polymer-casting solvent gives the polymer more time to crystallize and thus increases overall crystallinity.

We further quantified the crystalline domain sizes using the full width at half-maximum (fwhm) of the (100) peaks via the Scherrer equation (details in the SI). We note that in conjugated polymer systems like those studied here, the broadening of X-ray scattering peaks results from a combination of finite size effects, as seen in traditional crystalline materials, as well as disordered-induced broadening. As a result, domain sizes derived from the fwhm of diffraction peaks using the Scherrer equation correspond to what we call the crystalline coherence length, which is always smaller than or equal to the actual crystallite size because of the effects of chain packing disorder. Although there is an increase in overall crystallinity of the pure polymer upon the addition of DIO, the coherence length is unchanged within the error, going from 4.1 nm for the pure polymer to 3.7 nm with DIO (Table S1 of the SI).

We next examined the results of removing the DIO additive from the pure polymer films. Because it is detrimental to device performance, several groups have investigated removing DIO

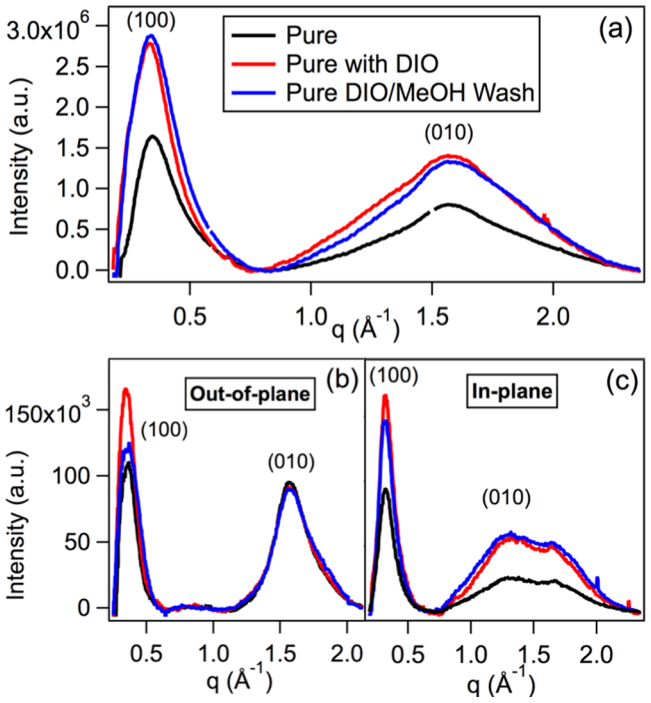


**Figure 2.** (a) Full integration of GIWAXS diffractograms for pure polymer films showing the increase in crystallinity with the addition of DIO, where the black curves are pure polymer, red curves are polymer with 3% DIO, and blue curves are obtained after washing the DIO away with methanol. The face-on orientation shown by the strong (010) diffraction in the out-of-plane direction (b), with much less intensity in-plane direction (c).

from BHJ active layers using techniques such as the application of high vacuum[71,72] or methanol washing.[68−72] In particular, Ye and co-workers showed that by monitoring the C−I stretch vibrations from DIO, both techniques can remove DIO from PBDTTT-C:PCBM BHJs with similar efficacy.[71] Here, we remove the DIO from our films via methanol washing, as this provides consistency between our GIWAXS and device active layer samples. For the pure polymer films, we found that methanol washing produced very little change in the structure of films cast with DIO as a solvent additive. The calculated Scherrer length of 3.8 nm is very close to that of the polymer film with DIO and still within the error of the pure polymer. Indeed, neither methanol nor the 2CP:DCM solvent blend that we used for casting the fullerene during SqP significantly changed overall the polymer crystallinity or chain orientation (see Figure S1 of the SI).

We next determined the extent of the polymer chain orientation in the pure polymer films by directionally integrating the diffractograms. To look at the orientation, we took 10° integration slices in the out-of-plane (Figure 2b) and in-plane (Figure 2c) directions. By comparing the out-of-plane and in-plane peaks, it is apparent that the PBDTTT-C chains in pure films lie mostly face-on. The face-on orientation can be determined from the (010) $\pi-\pi$-stacking peak, which appears at 1.57 $Å^{-1}$ in the out-of-plane patterns. The high out-of-plane intensity relative to the in-plane intensity is indicative of a face-on chain orientation. We note that the relative (010) peak intensity is a better measure of chain orientation than the relative (100) peak intensity because of interference from the specular reflection in the (100) peaks. Although we always subtract the specular reflection away before integration, its



DOI: 10.1021/acs.jpcc.8b02859
J. Phys. Chem. C 2018, 122, 15078−15089

intensity varies with surface roughness, so perfect background subtractions are not always possible. We note that for all samples, the in-plane (010) peak is much broader than the out-of-plane peak and is dominated by a shoulder shifted to lower $q$ (centered at about 1.3 Å$^{-1}$). The shoulder indicates the presence of some disordered, edge-on polymer chains that have a significantly larger $\pi-\pi$-stacking distance. Thus, although the chains in the pure film are not perfectly face-on oriented, the data show that PBDTTT-C films do have an excess of face-on domains and that those face-on domains appear to be more ordered.

The orientation of the pure polymer chains is mostly maintained upon addition of DIO, whose dominant effect is to produce an increase in overall crystallinity, as observed in Figure 2b. This increase in crystallinity is likely due to the slower drying kinetics with DIO, since its low vapor pressure causes it to remain in the film.[76] Some decrease in face-on orientation is also observed with DIO addition as indicated by the relative increase in the in-plane (010) scattering intensity. No significant additional changes are observed upon removing the DIO with methanol. Overall, these data suggest that pure PBDTTT-C, without additives, is the most promising candidate for devices that require a face-on polymer orientation but that DIO-containing films still show a significant fraction of face-on polymer chains for such applications.

*B. Polymer Orientation in Blend-Cast PBDTTT-C BHJs with PCBM.* Now that we have an understanding of the chain conformation in pure PBDTTT-C films, we turn to assessing whether or not this orientation is maintained during blend-casting with PCBM. The fully integrated diffractograms for blend-cast BHJs are shown in Figure 3a, which can be compared to the pure polymer patterns in Figure 2a. The data show both the (100) lamellar polymer diffraction at 0.36 Å$^{-1}$ and several $PC_{71}BM$ scattering peaks located at 0.66, 1.34, and 1.89 Å$^{-1}$. In addition to increasing the polymer crystallinity, the use of DIO as a solvent additive in BC devices also decreases the lamellar (100) polymer peak width, indicating the formation of larger crystalline PBDTTT-C domains.[49,62] Indeed, the calculated coherence length increases from 2.4 to 3.9 nm upon the addition of DIO to the BC film without a significant change in overall crystallinity. Increased domain size, up to a certain extent, can enable better hole conductivity through the polymer network and is likely partially responsible for the increase in current observed for the DIO-treated blend-cast BHJ devices, whose properties are discussed below.

Unlike the case for the pure polymer films, we do see significant changes in the scattering from DIO-containing blend-cast BHJ films upon washing with methanol. After methanol washing, we are left with higher overall crystallinity and similar Scherrer domain sizes of 3.1 nm. Further, methanol washing causes a significant increase in the fullerene crystallinity as seen by the increase in the intensity of the peak centered at about 1.3 Å$^{-1}$ in Figure 3a. The removal of DIO with methanol washing clearly enables the polymer:-fullerene system to pack better and form more crystalline domains, creating a better overall bicontinuous BHJ network. We note that in addition to removing the DIO, the methanol wash likely also removes any residual blend-casting solvent. This conclusion is based on the fact that methanol washing a blend-cast film without any DIO additive (shown in Figure S2 of the SI) also produces a slight increase in fullerene crystallinity, though this increase is to a much smaller extent than in BHJ films prepared with DIO.

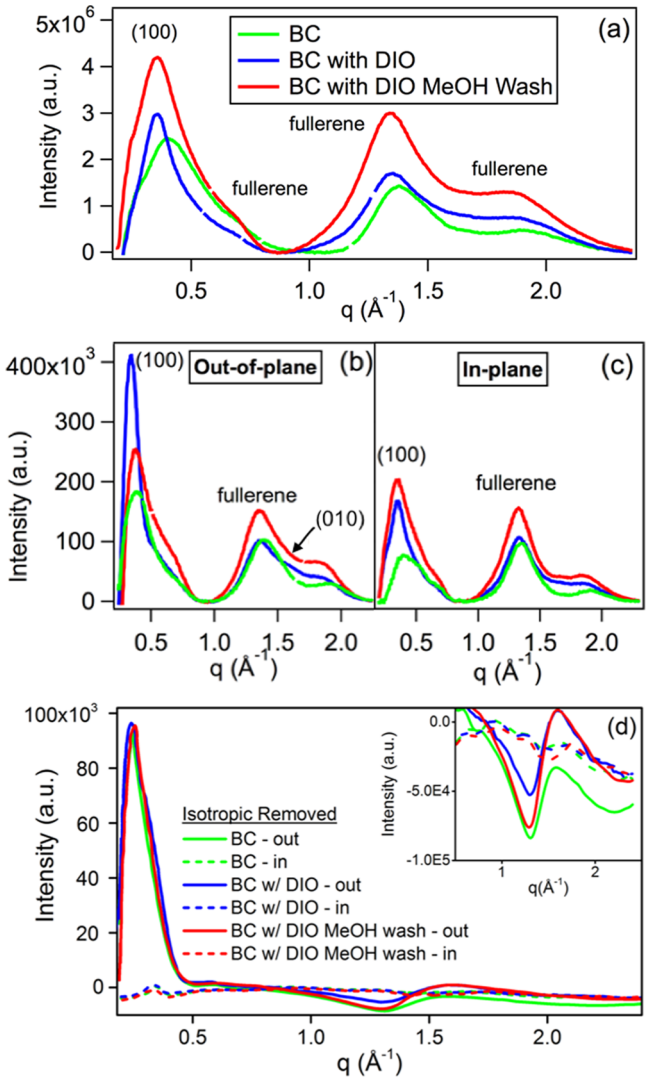


**Figure 3.** (a) Full integrations of GIWAXS diffractograms for 1:1.5 PBDTTT-C:PCBM blend-cast films without DIO (green), with 3% DIO (blue), and methanol washed (red). The films appear to show a preference for an edge-on polymer chain orientation, as seen by the strong (100) scattering in the (b) out-of-plane direction but not in the (c) in-plane direction. Examination of the (010) scattering in (d) in both the out-of-plane and in-plane diffractions is facilitated by subtraction of all isotropic scattering, which includes the fullerene diffraction. The inset in (d) is a zoom-in of the (010) polymer region and shows negative intensities in the out-of-plane direction, which again indicates a lack of face-on polymer chains.

We also compared the in-plane and out-of-plane diffraction of our blend-cast BHJs to determine the average polymer domain orientation, as plotted in Figure 3b,c. In these panels, we see a large out-of-plane (100) lamellar-stacking peak with a correspondingly much smaller in-plane lamellar diffraction. This suggest that the PBDTTT-C polymer in blend-cast BHJs has an orientation that is more edge-on or isotropic, rather than mostly face-on, as observed for the pure polymer. Because of potential interference form the specular reflection, however, it would make sense to confirm this conclusion using the (010) diffraction peak. Unfortunately, the (010) $\pi-\pi$-stacking peak in these BHJs is largely obscured by the presence of the strong,


DOI: 10.1021/acs.jpcc.8b02859
J. Phys. Chem. C 2018, 122, 15078−15089

isotropic fullerene scattering centered at 1.34 $Å^{-1}$. For the sample with DIO, the (010) peak is observed as a small shoulder, but the intensity in both samples is too small for quantitative analysis. To extract the (010) $\pi-\pi$-stacking peak from the fullerene peak, we took a 10° radial segment from the diffractogram centered at 45°, which contains scattering from any peaks with an isotropic orientation. Since the fullerene diffraction is isotropic, we subtracted the 45° segment from both the out-of-plane and in-plane data in Figures 3b,c, respectively. This procedure should leave only the nonisotropic polymer diffraction. The results of this subtraction procedure are shown in Figure 3d, where we see that the (100) lamellar peak for the blend-cast film now lies entirely out-of-plane. This indicates that no polymer domains show a preference for face-on orientation and that indeed most of the blend-cast sample is isotropic.

We next focus on the (010) $\pi-\pi$-scattering region; here, the subtracted data are quite complex. In the in-plane direction, little nonisotropic scattering is observed. In the out-of-plane direction, by contrast, we see a derivative-shaped peak. The negative intensity of this peak indicates a lack of face-on oriented polymer chains relative to the isotropic scattering, and the overall derivative shape indicates that those chains that do orient face-on have a slightly different lattice spacing than the isotropic chains. As discussed above, we frequently observe this trend, with a smaller $\pi$-stacking distance in face-on chains that are flattened by interaction with the substrate. The combination of increased out-of-plane lamellar diffraction and decreased out-of-plane $\pi$-stacking intensity thus indicates that for blend-cast films without DIO, the polymer no longer has a net face-on orientation.

Finally, we can compare the blend-cast BHJ films with and without the DIO additive. When DIO is used in the casting solution, the (100) lamellar peak intensity increases in both the in-plane and out-of-plane directions, indicating greater overall crystallinity, as discussed above. A small out-of-plane (010) peak can also be seen between the two fullerene diffraction peaks at ~1.6 $Å^{-1}$, which was not visible in the blend-cast sample without DIO. The existence of this out-of-plane (face-on) (010) peak is confirmed in the 45°-subtracted curve, which again shows no signal in the in-plane direction, but now shows some positive intensity in the out-of-plane direction (Figure 3c). This indicates a slightly larger population of a face-on oriented polymer chains for the films cast with DIO. A loss of out-of-plane isotropic (010) scattering and an increase in face-on out-of-plane (010) scattering are also observed for methanol-washed samples, this time accompanied by a relative increase in the in-plane (100) scattering, indicating even further recovery of the face-on orientation in the methanol washed samples and the highest overall crystallinity out of all our conditions. The recovery of face-on orientation and increased coherence length, in combination with the increased overall crystallinity, explains the higher current and increased overall performance observed in blend-cast devices made with DIO (removed by methanol washing) as discussed in more detail below.

*C. Polymer Orientation in Sequentially Processed PBDTTT-C BHJs with PCBM.* One goal in using naturally face-on oriented polymers is to be able to preserve the favorable polymer orientation in BHJ devices blended with fullerene. We have shown above, however, that the face-on morphology is not always well-preserved by blend-casting; the presence of fullerene during film formation can kinetically frustrate crystallization, leading to isotropic polymer orientation. The use of low-vapor-pressure solvents like DIO leaves the film wet with solvent for an extended period of time, partly alleviating the frustration. But an alternative to preserving face-on polymer domain orientation in BHJs is to use sequential processing, where a pure polymer layer is deposited first with a face-on orientation, and then, the fullerene is infiltrated in a second step using a solvent that swells but does not dissolve the underlying polymer film. We have argued in previous work that SqP preserves much of the morphology of the original polymer film,[24,25,33,77,78] so it is entirely possible that the method could better preserve the native polymer orientation producing real differences in the net orientation of blend-cast and sequentially processed BHJs of the same materials.

Figure 4a shows radially integrated two-dimensional GIWAXS diffractograms for sequentially processed films with and without DIO additive in the polymer-casting solution. It should be noted that the PCBM concentration used for these films was 5 mg/mL, whereas the optimal PCBM concentration for sequentially processed photovoltaic devices is 10 mg/mL. The GIWAXS data for films made with 10 mg/mL PCBM are shown in Figure S3 of the SI, where the large fullerene peaks with the high fullerene concentration make the analysis of these patterns difficult. The increased fullerene peak intensity is consistent with the fact that the optimized SqP device has a PBDTTT-C:$PC_{71}BM$ weight ratio of 1:3.5 (see SI, Figure S4), much higher than the BC ratio of 1:1.5. Therefore, we choose to analyze the GIWAXS data for the 5 mg/mL PCBM sequentially processed samples, where the trends in the various peaks are easier to extract.

We note that in SqP, because the vapor pressure of DIO is low, if DIO is used in the polymer-casting solution, some of it remains in the film during the fullerene deposition stage. Figure 4a shows that the addition of DIO to the polymer-casting solution does not significantly change the overall crystallinity; however, it does increase the coherence length from 4.9 to 5.7 nm. Since the coherence lengths are larger than both the pure polymer films and the blend-cast BHJ films, we performed photoluminescence (PL) quenching experiments to verify that the sequentially processed films still were sufficiently mixed to provide good exciton harvesting. Figure 5 shows the PL of PBDTTT-C films fabricated via BC and SqP with and without DIO. The intensity was scaled by the polymer absorption at the excitation wavelength (see Figure S5 in the SI), and the data show that in all cases, the BHJ films' PL is more than 90% quenched compared to pure PBDTTT-C. The PL data thus confirms that there is adequate polymer:fullerene mixing for BHJ films made via both processing methods, despite the larger domain sizes obtained via SqP. In fact, Figure 5 shows that the blend-cast-with-DIO film has the most residual PL, which makes sense as it has the highest overall crystallinity (see Table S1 of the SI).

The presence of DIO in the polymer-casting solution also causes an increase in the intensity of the $PC_{71}BM$ scattering peak centered at 1.34 $Å^{-1}$ as seen in Figure 4. This intensity increase suggests that DIO enables $PC_{71}BM$ to diffuse more easily into the polymer, which likely occurs because of the low vapor pressure of DIO,[57,65] resulting in some DIO remaining in the film under ambient conditions.[63] As a result, the film is still partially wet with DIO during the fullerene-casting step in SqP. Favorable mixing between DIO and the SqP-casting solvent then results in DIO-induced polymer swelling.[70] Increased solvent swelling during SqP either allows more


DOI: 10.1021/acs.jpcc.8b02859
J. Phys. Chem. C 2018, 122, 15078−15089

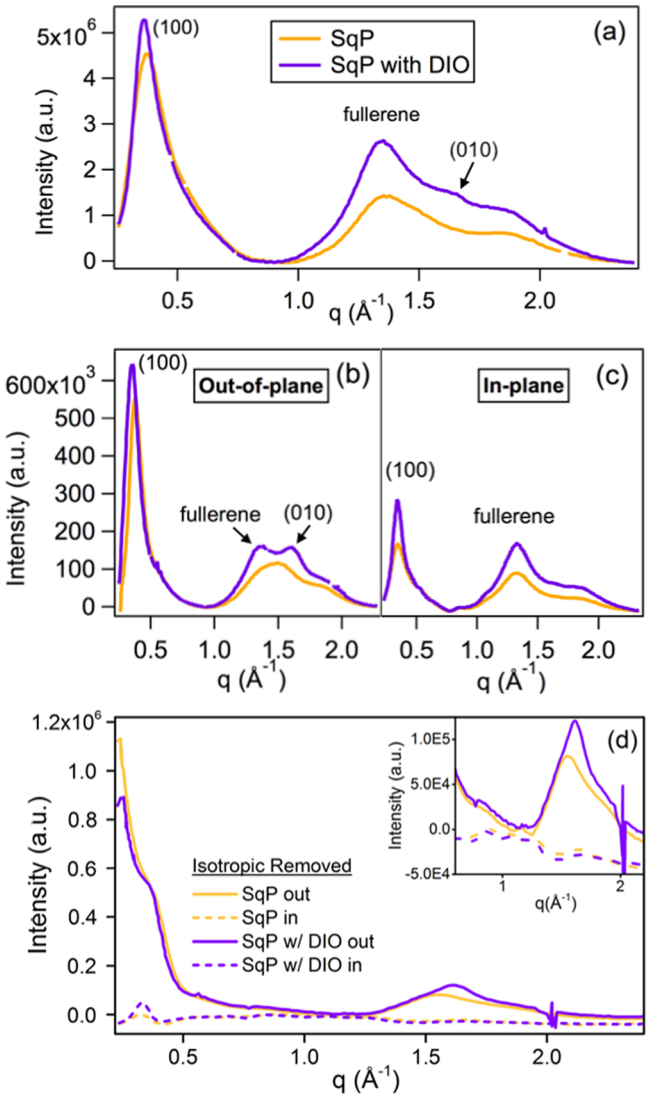


**Figure 4.** (a) Full integration of GIWAXS diffractograms for sequentially processed (SqP) PBDTTT-C:PCBM films, where the orange curves have no additive, and the purple curves have 3% DIO in the polymer-casting solution. Despite the fullerene scattering, strong (010) diffraction can be seen in the out-of-plane scattering in part (b), but not in the in-plane scattering in part (c). Examination of the (010) scattering in (d) in both the out-of-plane and in-plane diffractions is again facilitated by subtraction of all isotropic scattering, which includes the fullerene diffraction. The inset in (d) is a zoom-in of the (010) polymer region and shows strong positive intensities in the out-of-plane direction, indicative of a face-on polymer chain alignment.

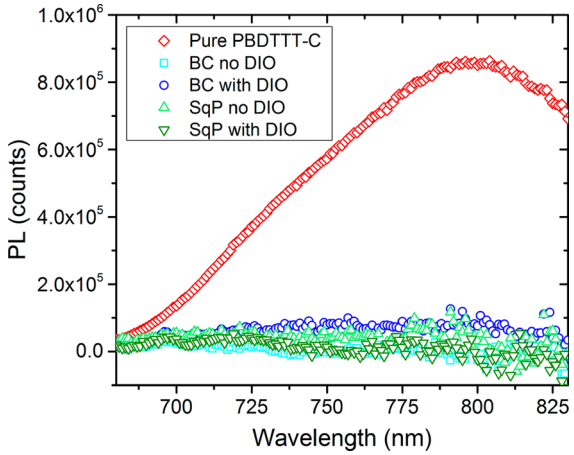


**Figure 5.** Photoluminescence of pure PBDTTT-C (red squares) as well as BHJ films made via BC with DIO (dark blue circles) and without DIO (light blue squares), SqP with DIO (dark green down triangles) and without DIO (light green up triangles). A methanol wash was performed to remove the DIO in the BC case, while in SqP, we rely on the SqP solvents to remove the DIO. The PL intensities have been normalized by the polymer optical density at the excitation wavelength (630 nm, see SI Figure S5). All of the BHJs are well-quenched, indicating the domains in the films are well-mixed.

fullerene to incorporate into the film or allows whatever fullerene that is present in the film to become more crystalline, both of which result in increased fullerene diffraction and could be beneficial for device performance.

In contrast to the blend-cast BHJ films, the in- and out-of-plane diffractograms for the sequentially processed BHJ films (Figure 4b,c) show more pronounced differences in scattering intensity. The data clearly show a (010) scattering peak (shoulder) in the out-of-plane direction but not in the in-plane direction for the sequentially processed films made both with and without DIO. The presence of this strong out-of-plane $\pi-\pi$ peak means that PBDTTT-C in the sequentially processed BHJs is far more face-on than in its blend-cast counterparts. There is also somewhat more (100) lamellar scattering intensity observed in the in-plane direction for the sequentially processed BHJs than was seen with the blend-cast BHJ films, consistent with a more face-on domain orientation.

Although the (010) polymer diffraction peaks can be seen in the sequentially processed samples, strong fullerene diffraction again makes quantitative analysis difficult, so as with the analysis above, Figure 4d shows the results of subtracting off the isotropic diffraction measured at 45°. Unlike the blend-cast films, where the subtraction led to a derivative shape, the sequentially processed PBDTTT-C:$PC_{71}BM$ BHJs instead show a distinct peak in the (010) region for out-of-plane scattering (inset of Figure 4d). Moreover, the (100) lamellar scattering in the sequentially processed BHJs shows more in-plane intensity than in the blend-cast samples, again indicating a more face-on orientation. Thus, in contrast to blend-cast BHJs, SqP-based devices have stronger face-on polymer orientation both with and without DIO, similar to pure polymer samples.

**II. Device Performance of Blend-Cast and Sequentially Processed PBDTTT-C:$PC_{71}BM$ BHJs.** To understand how all of the above structural observations affect actual device performance, we fabricated OPVs with blend-cast and sequentially processed PBDTTT-C:$PC_{71}BM$ active layers, without DIO, with DIO, and with DIO removed via methanol treatment; the results are summarized in Figure 6 and Table 1. To further correlate performance with variations in mobility as a result of changes in polymer orientation and degree of crystallinity, we fabricated hole-only diodes and fit the corresponding dark $J-V$ curves to the space-charge-limited current (SCLC) model, yielding the hole mobilities listed in Table 2. Details of the fitting procedure and corresponding fits to the data are shown in Figure S6 of the SI.

As has been observed in previous work,[60−62] the addition of DIO during blend-casting is necessary for optimal device performance. Our blend-cast photovoltaic device data fits with this expectation, as we observe an increase in overall power


DOI: 10.1021/acs.jpcc.8b02859
J. Phys. Chem. C 2018, 122, 15078−15089

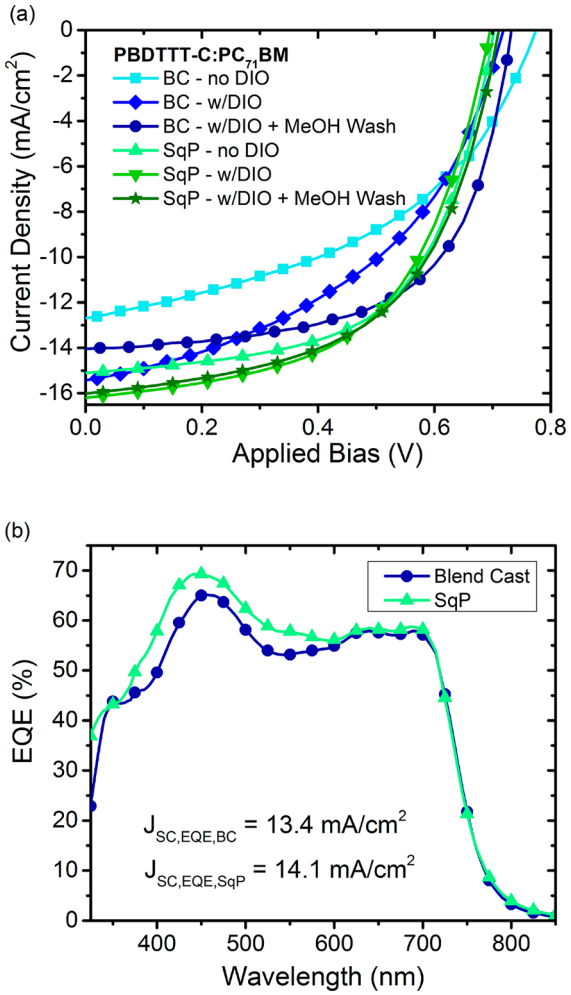


**Figure 6.** (a) $J-V$ device curves for blend-cast films without additives (light blue squares) and with 3% v/v DIO (blue diamonds). Additional improvement is seen with methanol washing the DIO films (dark blue circles). Sequential processing without the use of additives (light green triangles) shows improvement over the blend-cast films, mainly due to Jsc improvement. SqP devices fabricated with 3% v/v DIO (green down triangles) and, subsequently, MeOH washed (dark green stars) are similar in performance to SqP devices without additives. All devices have the structure: ITO/PEDOT:PSS/PBDTTT-C:$BC_{71}$BM:Ca/Al. (b) External quantum efficiency (EQE) for optimized blend-cast (w/DIO + MeOH wash) and sequentially processed films (no additional processing), showing higher obtainable current with SqP.

conversion efficiency from 4.4 to 5.0% upon the addition of 3% DIO by volume (Figure 6a and Table 1). The boost in efficiency arises from a slight improvement in the fill factor and a large improvement in the short-circuit current, $J_{SC}$, from 12.7 to 15.4 mA/cm$^2$ for devices without and with DIO, respectively. Upon washing the blend-cast-with-DIO films with methanol, the PCE is further increased to 6.3%. These results fit well with the observed SCLC hole mobility increase from $2.8 \times 10^{-5}$ cm$^2$V$^{-1}$s$^{-1}$ in the blend-cast active layer to $1.26 \times 10^{-4}$ cm$^2$V$^{-1}$s$^{-1}$ in the optimized blend-cast films with DIO and subsequent methanol wash. On the basis of the scattering data in Figures 1 and 3, we associate the improvement in mobility when DIO is added to a combination of increased polymer face-on orientation and an increase in domain size. DIO removal further causes an increase in crystallinity and more favorable rearrangement of the fullerene, as discussed above, and also eliminates any detrimental effects DIO might have on device performance.[70−72]

Although we expected an increase in PCE with the use of DIO for blend-cast systems, surprisingly, we see similarly high PCEs for devices fabricated via SqP, both with and without DIO. Without the use of any additives, SqP produces a higher $J_{SC}$ than the optimized blend-cast devices, which is verified by the external quantum efficiency (EQE) measurements shown in Figure 5b; the EQE curves, when integrated, yield the measured short-circuit currents to within a few percent. We note that a similar improvement in $J_{SC}$ with SqP compared to BC has been seen with a related polymer, PBDTTT-C-T.[21] In the case of PBDTTT-C-T, however, the $J_{SC}$ improvement was attributed to improved vertical phase separation with SqP rather than to changes in the polymer domain orientation, as we postulate here. The higher $J_{SC}$ for SqP devices is consistent with the higher hole mobility expected through the stacked $\pi$-conjugation. Indeed, the SCLC hole mobility for the optimized SqP active layer (without DIO) is $2.9 \times 10^{-4}$ cm$^2$V$^{-1}$s$^{-1}$, an order of magnitude higher than that of the blend-cast device without DIO and more than twice that of the optimized blend-cast device (with DIO and methanol wash). Since the overall crystallinity is lower in the SqP device compared to the optimized BC, the mobility improvement can be assuredly attributed to polymer orientation effects.

In contrast to the blend-cast films, neither the addition of DIO to the polymer layer nor subsequent methanol washing has a significant effect on the overall performance of

**Table 2. SCLC Hole Mobilities ($\mu_{hole}$)[a,b]**

| active layer | $\mu_{hole}$ (cm$^2$V$^{-1}$s$^{-1}$) |
|---|---|
| pure PBDTTT-C | $1.07(6) \times 10^{-3}$ |
| sequentially processed | $2.9(2) \times 10^{-4}$ |
| blend-cast | $1.26(8) \times 10^{-4}$ |
| blend-cast no DIO | $2.8(2) \times 10^{-5}$ |

[a]Representative active layers: pure PBDTTT-C, optimized SqP (without DIO), optimized BC (with DIO and MeOH wash), and BC without DIO. [b]The results for the pure polymer and optimized blend-cast are in agreement with the literature.[57,62,79]

**Table 1. Summary of $J-V$ Characteristics for the Devices Shown in Figure 5[a]**

| device | | $V_{oc}$ (V) | $J_{sc}$ (mA/cm$^2$) | FF (%) | PCE (%) |
|---|---|---|---|---|---|
| blend-cast | no DIO | 0.775 ± 0.005 | −12.7 ± 0.2 | 45 ± 4 | 4.4 ± 0.5 |
| | with 3% v/v DIO | 0.719 ± 0.004 | −15.4 ± 0.4 | 46 ± 3 | 5.0 ± 0.4 |
| | with 3% v/v DIO + MeOH wash | 0.733 ± 0.005 | −14.0 ± 0.5 | 61 ± 2 | 6.3 ± 0.3 |
| sequentially processed | no DIO | 0.701 ± 0.006 | −15.1 ± 0.6 | 59 ± 3 | 6.3 ± 0.4 |
| | with 3% v/v DIO | 0.711 ± 0.003 | −16.0 ± 0.8 | 56 ± 1 | 6.3 ± 0.2 |
| | with 3% v/v DIO + MeOH wash | 0.696 ± 0.005 | −16.2 ± 0.6 | 55 ± 2 | 6.2 ± 0.3 |

[a]The device characteristics were averaged over 3 films (12 devices) and are presented with ± the standard deviation of each set of conditions.



DOI: 10.1021/acs.jpcc.8b02859
J. Phys. Chem. C 2018, 122, 15078−15089

sequentially processed devices. As discussed above, the addition of DIO to the polymer-casting solution for SqP devices does lead to slightly larger domain sizes, but the Scherrer domain sizes and extent of face-on orientation remain relatively unchanged, in sharp contrast to the role of DIO in blend-cast devices. The lack of appreciable change in the PCE indicates that this slight increase in fullerene content and/or crystallinity with DIO is not important for device performance. Furthermore, methanol washing is no longer necessary, as it has no significant effect on the device performance, likely because the solvent blend used in the SqP step already washes any excess DIO out of the active layer. Thus, sequentially processed devices do not need processing additives (or a subsequent methanol wash) to match the optimized 6.3% PCE of the blend-cast system, which requires both DIO and a subsequent washing step. Given that all BHJ morphologies are adequately mixed and that the overall crystallinity is lower in sequentially processed samples than in blend-cast devices, the preservation of the face-on orientation of PBDTTT-C in sequentially processed films must be the main contributor to performance enhancements.

## CONCLUSIONS

In this work, we have shown that the face-on orientation of pure PBDTTT-C films is not preserved when standard blend-casting techniques for creating polymer:fullerene BHJs are employed. Although PBDTTT-C shows a preferred face-on orientation in pure films, regardless of the presence of any solvent additive, the interactions of the polymer with $PC_{71}BM$ appear to dominate over polymer−substrate interactions, leading to a loss of the natural face-on polymer orientation upon blended film formation. The addition of DIO helps to restore the face-on tendency of the domains in this material when blend-casting.

By producing BHJ devices from PBDTTT-C using sequential processing, however, the face-on orientation of the pure polymer film can be preserved even without additives, as summarized in the TOC graphic. Sequential processing thus enables us to translate pure polymer properties into blended BHJ devices. The benefits of preserving the face-on polymer orientation are seen in improved hole mobility and overall device performance. Face-on orientation enables more efficient hole conduction through the polymer $\pi$-system, yielding a higher $J_{SC}$ in OPV devices. Overall, even though the final device performance for this polymer:fullerene combination is similar for blend-cast and sequentially processed devices, the structure of the polymer in the two devices is quite different. We note that although the focus of this work is on the preservation of optimized polymer chain orientations using solvent additives or SqP, an interesting corollary is the observation of the remarkable flexibility of the BHJ morphology: we see that there are a wide range of underlying BHJ architectures that can lead to good device performance, which perhaps explains why the BHJ concept works so well in the first place.[24] In the PBDTTT-C blend-cast system, we see higher overall crystallinity but smaller crystalline domains, whereas SqP produces BHJs with lower overall crystallinity but domains that are larger and more face-on oriented. When optimized, both techniques can lead to good device performance.

Overall, our work emphasizes that these two distinct processing methods for creating OPV active layers can be used to enhance different aspects of polymer structure and nanoscale morphology. By adding SqP alongside BC with solvent additives to the OPV processing toolbox, researchers now have a larger variety of ways to robustly and reproducibly tune both polymer crystallinity and domain orientation in semiconducting polymer OPV devices.

## ASSOCIATED CONTENT

### Supporting Information

The Supporting Information is available free of charge on the ACS Publications website at DOI: 10.1021/acs.jpcc.8b02859.

Details of device fabrication including electrode deposition, summary table of parameters from GIWAXS, 2D GIWAXS diffractograms, BC redissolved film absorbance, all film absorbance, dark $J-V$ curves with details of SCLC fits for extracting hole mobilities, $J-V$ curves with DIO in different steps of the SqP process (PDF)

## AUTHOR INFORMATION


### Corresponding Authors

*E-mail: tolbert@chem.ucla.edu (SHT)
*E-mail: schwartz@chem.ucla.edu (BJS)

### ORCID

Benjamin J. Schwartz: 0000-0003-3257-9152
Sarah H. Tolbert: 0000-0001-9969-1582


### Author Contributions

‖TJA and ASF contributed equally to this work.

### Notes

The authors declare no competing financial interest.

## ACKNOWLEDGMENTS

The authors would like to acknowledge Matthew Voss for helpful discussions concerning the PL measurements. This work was supported by the National Science foundation under grant CHE-1608957. The X-ray diffraction studies presented in this manuscript were carried out at the Stanford Synchrotron Radiation Lightsource. Use of the Stanford Synchrotron Radiation Lightsource, SLAC National Accelerator Laboratory, is supported by the U.S. Department of Energy, Office of Science, Office of Basic Energy Sciences, under Contract DE-AC02-76SF00515.

## REFERENCES


(1) Green, M. A.; Emery, K.; Hishikawa, Y.; Warta, W.; Dunlop, E. D. Solar Cell Efficiency Tables (Version 43). *Prog. Photovoltaics* **2014**, *22*, 1−9.

(2) He, Z.; Zhong, C.; Su, S.; Xu, M.; Wu, H.; Cao, Y. Enhanced Power-Conversion Efficiency in Polymer Solar Cells Using an Inverted Device Structure. *Nat. Photonics* **2012**, *6*, 591−595.

(3) Zhao, J.; Li, Y.; Yang, G.; Jiang, K.; Lin, H.; Ade, H.; Ma, W.; Yan, H. Efficient Organic Solar Cells Processed from Hydrocarbon Solvents. *Nat. Energy* **2016**, *1*, 15027.

(4) Collins, B. A.; Tumbleston, J. R.; Ade, H. Miscibility, Crystallinity, and Phase Development in P3HT/PCBM Solar Cells: Toward an Enlightened Understanding of Device Morphology and Stability. *J. Phys. Chem. Lett.* **2011**, *2*, 3135−3145.

(5) Halls, J. J. M.; Walsh, C. A.; Greenham, N. C.; Marseglia, E. A.; Friend, R. H.; Moratti, S. C.; Holmes, A. B. Efficient Photodiodes from Interpenetrating Polymer Networks. *Nature* **1995**, *376*, 498−500.

(6) Shaheen, S. E.; Brabec, C. J.; Serdar Sariciftci, N.; Padinger, F.; Fromherz, T.; Hummelen, J. C. 2.5% Efficient Organic Plastic Solar Cells. *Appl. Phys. Lett.* **2001**, *78*, 841−843.




DOI: 10.1021/acs.jpcc.8b02859
J. Phys. Chem. C 2018, 122, 15078−15089

(7) Shaw, P. E.; Ruseckas, A.; Samuel, I. D. W. Exciton Diffusion Measurements in Poly(3-Hexylthiophene). *Adv. Mater.* **2008**, *20*, 3516−3520.
(8) Yu, G.; Gao, J.; Hummelen, J. C.; Wudl, F.; Heeger, A. J. Polymer Photovoltaic Cells: Enhanced Efficiencies via a Network of Internal Donor-Acceptor Heterojunctions. *Science* **1995**, *270*, 1789−1791.
(9) Peet, J.; Soci, C.; Coffin, R. C.; Nguyen, T. Q.; Mikhailovsky, A.; Moses, D.; Bazan, G. C. Method for Increasing the Photoconductive Response in Conjugated Polymer/Fullerene Composites. *Appl. Phys. Lett.* **2006**, *89*, 252105.
(10) Peet, J.; Kim, J. Y.; Coates, N. E.; Ma, W. L.; Moses, D.; Heeger, A. J.; Bazan, G. C. Efficiency Enhancement in Low-Bandgap Polymer Solar Cells by Processing with Alkane Dithiols. *Nat. Mater.* **2007**, *6*, 497−500.
(11) Lee, J. K.; Ma, W. L.; Brabec, C. J.; Yuen, J.; Moon, J. S.; Kim, J. Y.; Lee, K.; Bazan, G. C.; Heeger, A. J. Processing Additives for Improved Efficiency from Bulk Heterojunction Solar Cells. *J. Am. Chem. Soc.* **2008**, *130*, 3619−3623.
(12) Kwon, S.; Kang, H.; Lee, J.-H.; Lee, J.; Hong, S.; Kim, H.; Lee, K. Effect of Processing Additives on Organic Photovoltaics: Recent Progress and Future Prospects. *Adv. Energy Mater.* **2017**, *7*, 1601496.
(13) Zhao, Y.; Xie, Z.; Qu, Y.; Geng, Y.; Wang, L. Solvent-Vapor Treatment Induced Performance Enhancement of Poly(3-Hexylthiophene):Methanofullerene Bulk-Heterojunction Photovoltaic Cells. *Appl. Phys. Lett.* **2007**, *90*, 043504−043506.
(14) Jo, J.; Na, S.-I.; Kim, S.-S.; Lee, T.-W.; Chung, Y.; Kang, S.-J.; Vak, D.; Kim, D.-Y. Three-Dimensional Bulk Heterojunction Morphology for Achieving High Internal Quantum Efficiency in Polymer Solar Cells. *Adv. Funct. Mater.* **2009**, *19*, 2398−2406.
(15) Ma, W.; Yang, C.; Gong, X.; Lee, K.; Heeger, A. J. Thermally Stable, Efficient Polymer Solar Cells with Nanoscale Control of the Interpenetrating Network Morphology. *Adv. Funct. Mater.* **2005**, *15*, 1617−1622.
(16) Kim, K.; Liu, J.; Namboothiry, M. A. G.; Carroll, D. L. Roles of Donor and Acceptor Nanodomains in 6% Efficient Thermally Annealed Polymer Photovoltaics. *Appl. Phys. Lett.* **2007**, *90*, 163511.
(17) Verploegen, E.; Mondal, R.; Bettinger, C. J.; Sok, S.; Toney, M. F.; Bao, Z. Effects of Thermal Annealing upon the Morphology of Polymer-Fullerene Blends. *Adv. Funct. Mater.* **2010**, *20*, 3519−3529.
(18) Ayzner, A. L.; Tassone, C. J.; Tolbert, S. H.; Schwartz, B. J. Reappraising the Need for Bulk Heterojunctions in Polymer−Fullerene Photovoltaics: The Role of Carrier Transport in All-Solution-Processed P3HT/PCBM Bilayer Solar Cells. *J. Phys. Chem. C* **2009**, *113*, 20050−20060.
(19) Gevaerts, V. S.; Koster, L. J. A.; Wienk, M. M.; Janssen, R. A. J. Discriminating Between Bilayer and Bulk Heterojunction Polymer:-Fullerene Solar Cells Using the External Quantum Efficiency. *ACS Appl. Mater. Interfaces* **2011**, *3*, 3252−3255.
(20) Moon, J. S.; Takacs, C. J.; Sun, Y.; Heeger, A. J. Spontaneous Formation of Bulk Heterojunction Nanostructures: Multiple Routes to Equivalent Morphologies. *Nano Lett.* **2011**, *11*, 1036−1039.
(21) Cheng, P.; Hou, J.; Li, Y.; Zhan, X. Layer-by-Layer Solution-Processed Low-Bandgap Polymer-PC61BM Solar Cells with High Efficiency. *Adv. Energy Mater.* **2014**, *4*, 1301349.
(22) Treat, N. D.; Brady, M. A.; Smith, G.; Toney, M. F.; Kramer, E. J.; Hawker, C. J.; Chabinyc, M. L. Interdiffusion of PCBM and P3HT Reveals Miscibility in a Photovoltaically Active Blend. *Adv. Energy Mater.* **2011**, *1*, 82−89.
(23) Ayzner, A. L.; Doan, S. C.; Tremolet De Villers, B.; Schwartz, B. J. Ultrafast Studies of Exciton Migration and Polaron Formation in Sequentially Solution-Processed Conjugated Polymer/Fullerene Quasi-Bilayer Photovoltaics. *J. Phys. Chem. Lett.* **2012**, *3*, 2281−2287.
(24) Hawks, S. A.; Aguirre, J. C.; Schelhas, L. T.; Thompson, R. J.; Huber, R. C.; Ferreira, A. S.; Zhang, G.; Herzing, A. A.; Tolbert, S. H.; Schwartz, B. J. Comparing Matched Polymer:Fullerene Solar Cells Made by Solution-Sequential Processing and Traditional Blend Casting: Nanoscale Structure and Device Performance. *J. Phys. Chem. C* **2014**, *118*, 17413−17425.
(25) Zhang, G.; Huber, R. C.; Ferreira, A. S.; Boyd, S. D.; Luscombe, C. K.; Tolbert, S. H.; Schwartz, B. J. Crystallinity Effects in Sequentially Processed and Blend-Cast Bulk-Heterojunction Polymer/Fullerene Photovoltaics. *J. Phys. Chem. C* **2014**, *118*, 18424−18435.
(26) Ferreira, A. S.; Aguirre, J. C.; Subramaniyan, S.; Jenekhe, S. A.; Tolbert, S. H.; Schwartz, B. J. Understanding How Polymer Properties Control OPV Device Performance: Regioregularity, Swelling, and Morphology Optimization Using Random Poly(3-Butylthiophene-Co-3-Octylthiophene) Polymers. *J. Phys. Chem. C* **2016**, *120*, 22115−22125.
(27) Schwenn, P. E.; Gui, K.; Nardes, A. M.; Krueger, K. B.; Lee, K. H.; Mutkins, K.; Rubinstein-Dunlop, H.; Shaw, P. E.; Kopidakis, N.; Burn, P. L.; et al. A Small Molecule Non-Fullerene Electron Acceptor for Organic Solar Cells. *Adv. Energy Mater.* **2011**, *1*, 73−81.
(28) Loiudice, A.; Rizzo, A.; Latini, G.; Nobile, C.; de Giorgi, M.; Gigli, G. Graded Vertical Phase Separation of Donor/acceptor Species for Polymer Solar Cells. *Sol. Energy Mater. Sol. Cells* **2012**, *100*, 147−152.
(29) Nardes, A. M.; Ayzner, A. L.; Hammond, S. R.; Ferguson, A. J.; Schwartz, B. J.; Kopidakis, N. Photoinduced Charge Carrier Generation and Decay in Sequentially Deposited Polymer/Fullerene Layers: Bulk Heterojunction vs Planar Interface. *J. Phys. Chem. C* **2012**, *116*, 7293−7305.
(30) Kim, D. H.; Mei, J.; Ayzner, A. L.; Schmidt, K.; Giri, G.; Appleton, A. L.; Toney, M. F.; Bao, Z. Sequentially Solution-Processed, Nanostructured Polymer Photovoltaics Using Selective Solvents. *Energy Environ. Sci.* **2014**, *7*, 1103.
(31) Aguirre, J. C.; Hawks, S. a.; Ferreira, A. S.; Yee, P.; Subramaniyan, S.; Jenekhe, S. A.; Tolbert, S. H.; Schwartz, B. J. Sequential Processing for Organic Photovoltaics: Design Rules for Morphology Control by Tailored Semi-Orthogonal Solvent Blends. *Adv. Energy Mater.* **2015**, *5*, 1402020.
(32) Liu, Y.; Liu, F.; Wang, H.; Nordlund, D.; Sun, Z.; Ferdous, S.; Russell, T. P. Sequential Deposition: Optimization of Solvent Swelling for High-Performance Polymer Solar Cells. *ACS Appl. Mater. Interfaces* **2015**, *7*, 653−661.
(33) Aguirre, J. C.; Hawks, S. A.; Ferreira, A. S.; Yee, P.; Subramaniyan, S.; Jenekhe, S. A.; Tolbert, S. H.; Schwartz, B. J. Sequential Processing for Organic Photovoltaics: Design Rules for Morphology Control by Tailored Semi-Orthogonal Solvent Blends. *Adv. Energy Mater.* **2015**, *5*, 1402020.
(34) Lee, K. H.; Schwenn, P. E.; Smith, A. R. G.; Cavaye, H.; Shaw, P. E.; James, M.; Krueger, K. B.; Gentle, I. R.; Meredith, P.; Burn, P. L. Morphology of All-Solution-Processed "Bilayer" Organic Solar Cells. *Adv. Mater.* **2011**, *23*, 766−770.
(35) Collins, B. A.; Gann, E.; Guignard, L.; He, X.; McNeill, C. R.; Ade, H. Molecular Miscibility of Polymer-Fullerene Blends. *J. Phys. Chem. Lett.* **2010**, *1*, 3160−3166.
(36) Tao, C.; Aljada, M.; Shaw, P. E.; Lee, K. H.; Cavaye, H.; Balfour, M. N.; Borthwick, R. J.; James, M.; Burn, P. L.; Gentle, I. R.; et al. Controlling Hierarchy in Solution-Processed Polymer Solar Cells Based on Crosslinked P3HT. *Adv. Energy Mater.* **2013**, *3*, 105−112.
(37) Piliego, C.; Holcombe, T. W.; Douglas, J. D.; Woo, C. H.; Beaujuge, P. M.; Fréchet, J. M. J. Synthetic Control of Structural Order in N -Alkylthieno[3,4-C]pyrrole-4,6-Dione-Based Polymers for Efficient Solar Cells. *J. Am. Chem. Soc.* **2010**, *132*, 7595−7597.
(38) Cabanetos, C.; El Labban, A.; Bartelt, J. A.; Douglas, J. D.; Mateker, W. R.; Fréchet, J. M. J.; McGehee, M. D.; Beaujuge, P. M. Linear Side Chains in Benzo[1,2-b:4,5-B′]dithiophene-thieno[3,4-c] Pyrrole-4,6-Dione Polymers Direct Self-Assembly and Solar Cell Performance. *J. Am. Chem. Soc.* **2013**, *135*, 4656−4659.
(39) Rivnay, J.; Steyrleuthner, R.; Jimison, L. H.; Casadei, A.; Chen, Z.; Toney, M. F.; Facchetti, A.; Neher, D.; Salleo, A. Drastic Control of Texture in a High Performance N-Type Polymeric Semiconductor and Implications for Charge Transport. *Macromolecules* **2011**, *44*, 5246−5255.


DOI: 10.1021/acs.jpcc.8b02859
*J. Phys. Chem. C* 2018, 122, 15078−15089

(40) Zhang, X.; Richter, L. J.; Delongchamp, D. M.; Kline, R. J.; Hammond, M. R.; McCulloch, I.; Heeney, M.; Ashraf, R. S.; Smith, J. N.; Anthopoulos, T. D.; et al. Molecular Packing of High-Mobility Diketo Pyrrolo-Pyrrole Polymer Semiconductors with Branched Alkyl Side Chains. *J. Am. Chem. Soc.* **2011**, *133*, 15073−15084.
(41) Liu, F.; Gu, Y.; Jung, J. W.; Jo, W. H.; Russell, T. P. On the Morphology of Polymer-Based Photovoltaics. *J. Polym. Sci., Part B: Polym. Phys.* **2012**, *50*, 1018−1044.
(42) Osaka, I.; Takimiya, K. Backbone Orientation in Semiconducting Polymers. *Polymer* **2015**, *59*, A1−A15.
(43) Saeki, A.; Koizumi, Y.; Aida, T.; Seki, S. Comprehensive Approach to Intrinsic Charge Carrier Mobility in Conjugated Organic Molecules, Macromolecules, and Supramolecular Architectures. *Acc. Chem. Res.* **2012**, *45*, 1193−1202.
(44) Ma, J.; Hashimoto, K.; Koganezawa, T.; Tajima, K. End-on Orientation of Semiconducting Polymers in Thin Films Induced by Surface Segregation of Fluoroalkyl Chains. *J. Am. Chem. Soc.* **2013**, *135*, 9644−9647.
(45) Lu, G. H.; Li, L. G.; Yang, X. N. Achieving Perpendicular Alignment of Rigid Polythiophene Backbones to the Substrate by Using Solvent-Vapor Treatment. *Adv. Mater.* **2007**, *19*, 3594−3598.
(46) Coakley, K. M.; Srinivasan, B. S.; Ziebarth, J. M.; Goh, C.; Liu, Y.; McGehee, M. D. Enhanced Hole Mobility in Regioregular Polythiophene Infiltrated in Straight Nanopores. *Adv. Funct. Mater.* **2005**, *15*, 1927−1932.
(47) Aryal, M.; Trivedi, K.; Hu, W. Nano-Confinement Induced Chain Alignment in Ordered P3HT Nanostructures Defined by Nanoimprint Lithography. *ACS Nano* **2009**, *3*, 3085−3090.
(48) Sirringhaus, H.; Brown, P. J.; Friend, R. H.; Nielsen, M. M.; Bechgaard, K.; Langeveld-Voss, B. M. W.; Spiering, A. J. H.; Janssen, R. A. J.; Meijer, E. W.; Herwig, P.; et al. Two-Dimensional Charge Transport in Self-Organized, High-Mobility Conjugated Polymers. *Nature* **1999**, *401*, 685−688.
(49) Hammond, M. R.; Kline, R. J.; Herzing, A. A.; Richter, L. J.; Germack, D. S.; Ro, H. W.; Soles, C. L.; Fischer, D. A.; Xu, T.; Yu, L.; et al. Molecular Order in High-Efficiency Polymer/Fullerene Bulk Heterojunction Solar Cells. *ACS Nano* **2011**, *5*, 8248−8257.
(50) Chen, M. S.; Niskala, J. R.; Unruh, D. A.; Chu, C. K.; Lee, O. P.; Fréchet, J. M. J. Control of Polymer-Packing Orientation in Thin Films through Synthetic Tailoring of Backbone Coplanarity. *Chem. Mater.* **2013**, *25*, 4088−4096.
(51) Osaka, I.; Kakara, T.; Takemura, N.; Koganezawa, T.; Takimiya, K. Naphthodithiophene−Naphthobisthiadiazole Copolymers for Solar Cells: Alkylation Drives the Polymer Backbone Flat and Promotes Efficiency. *J. Am. Chem. Soc.* **2013**, *135*, 8834−8837.
(52) Osaka, I.; Saito, M.; Koganezawa, T.; Takimiya, K. Thiophene-Thiazolothiazole Copolymers: Significant Impact of Side Chain Composition on Backbone Orientation and Solar Cell Performances. *Adv. Mater.* **2014**, *26*, 331−338.
(53) Szarko, J. M.; Guo, J.; Liang, Y.; Lee, B.; Rolczynski, B. S.; Strzalka, J.; Xu, T.; Loser, S.; Marks, T. J.; Yu, L.; et al. When Function Follows Form: Effects of Donor Copolymer Side Chains on Film Morphology and BHJ Solar Cell Performance. *Adv. Mater.* **2010**, *22*, 5468−5472.
(54) Proctor, C. M.; Love, J. A.; Nguyen, T.-Q. Mobility Guidelines for High Fill Factor Solution-Processed Small Molecule Solar Cells. *Adv. Mater.* **2014**, *26*, 5957−5961.
(55) Chen, H.; Hou, J.; Zhang, S.; Liang, Y.; Yang, G.; Yang, Y.; Yu, L.; Wu, Y.; Li, G. Polymer Solar Cells with Enhanced Open-Circuit Voltage and Efficiency. *Nat. Photonics* **2009**, *3*, 649−653.
(56) Hou, J.; Chen, H.-Y.; Zhang, S.; Chen, R. I.; Yang, Y.; Wu, Y.; Li, G. Synthesis of a Low Band Gap Polymer and Its Application in Highly Efficient Polymer Solar Cells. *J. Am. Chem. Soc.* **2009**, *131*, 15586−15587.
(57) Le Corre, V. M.; Chatri, A. R.; Doumon, N. Y.; Koster, L. J. A. Charge Carrier Extraction in Organic Solar Cells Governed by Steady-State Mobilities. *Adv. Energy Mater.* **2017**, *7*, 1701138.
(58) Chen, H. Y.; Lin, S. H.; Sun, J. Y.; Hsu, C. H.; Lan, S.; Lin, C. F. Morphologic Improvement of the PBDTTT-C and PC71BM Blend Film with Mixed Solvent for High-Performance Inverted Polymer Solar Cells. *Nanotechnology* **2013**, *24*, 484009.
(59) Hawks, S. A.; Deledalle, F.; Yao, J.; Rebois, D. G.; Li, G.; Nelson, J.; Yang, Y.; Kirchartz, T.; Durrant, J. R. Relating Recombination, Density of States, and Device Performance in an Efficient Polymer:Fullerene Organic Solar Cell Blend. *Adv. Energy Mater.* **2013**, *3*, 1201−1209.
(60) Ning, Y.; Lv, L.; Lu, Y.; Zhang, C.; Fang, Y.; Tang, A.; Hu, Y.; Lou, Z.; Teng, F.; Hou, Y. Effects of Photo-Induced Defects on the Performance of PBDTTT-C/PC70BM Solar Cells. *Phys. Status Solidi RRL* **2015**, *9*, 120−124.
(61) Yang, Y.; Chen, W.; Dou, L.; Chang, W.; Duan, H.; Bob, B.; Li, G.; Yang, Y. High-Performance Multiple-Donor Bulk Heterojunction Solar Cells. *Nat. Photonics* **2015**, *9*, 190−198.
(62) Zusan, A.; Gieseking, B.; Zerson, M.; Dyakonov, V.; Magerle, R.; Deibel, C. The Effect of Diiodooctane on the Charge Carrier Generation in Organic Solar Cells Based on the Copolymer PBDTTT-C. *Sci. Rep.* **2015**, *5*, 8286.
(63) Kong, J.; Song, S.; Yoo, M.; Lee, G. Y.; Kwon, O.; Park, J. K.; Back, H.; Kim, G.; Lee, S. H.; Suh, H.; et al. Long-Term Stable Polymer Solar Cells with Significantly Reduced Burn-in Loss. *Nat. Commun.* **2014**, *5*, 5688.
(64) Bijleveld, J. C.; Gevaerts, V. S.; Di Nuzzo, D.; Turbiez, M.; Mathijssen, S. G. J.; de Leeuw, D. M.; Wienk, M. M.; Janssen, R. A. J. Efficient Solar Cells Based on an Easily Accessible Diketopyrrolopyrrole Polymer. *Adv. Mater.* **2010**, *22*, E242−E246.
(65) Guo, X.; Zhang, M.; Ma, W.; Ye, L.; Zhang, S.; Liu, S.; Ade, H.; Huang, F.; Hou, J. Enhanced Photovoltaic Performance by Modulating Surface Composition in Bulk Heterojunction Polymer Solar Cells Based on PBDTTT-C-T/PC71BM. *Adv. Mater.* **2014**, *26*, 4043−4049.
(66) Chang, L.; Jacobs, I. E.; Augustine, M. P.; Moulé, A. J. Correlating Dilute Solvent Interactions to Morphology and OPV Device Performance. *Org. Electron.* **2013**, *14*, 2431−2443.
(67) Lou, S. J.; Szarko, J. M.; Xu, T.; Yu, L.; Marks, T. J.; Chen, L. X. Effects of Additives on the Morphology of Solution Phase Aggregates Formed by Active Layer Components of High-Efficiency Organic Solar Cells. *J. Am. Chem. Soc.* **2011**, *133*, 20661−20663.
(68) Li, N.; Brabec, C. J. Air-Processed Polymer Tandem Solar Cells with Power Conversion Efficiency Exceeding 10%. *Energy Environ. Sci.* **2015**, *8*, 2902−2909.
(69) Lu, L.; Yu, L. Understanding Low Bandgap Polymer PTB7 and Optimizing Polymer Solar Cells Based on It. *Adv. Mater.* **2014**, *26*, 4413−4430.
(70) Xiao, Z.; Yuan, Y.; Yang, B.; Vanderslice, J.; Chen, J.; Dyck, O.; Duscher, G.; Huang, J. Universal Formation of Compositionally Graded Bulk Heterojunction for Efficiency Enhancement in Organic Photovoltaics. *Adv. Mater.* **2014**, *26*, 3068−3075.
(71) Ye, L.; Jing, Y.; Guo, X.; Sun, H.; Zhang, S.; Zhang, M.; Huo, L.; Hou, J. Remove the Residual Additives Toward Enhanced Efficiency with Higher Reproducibility in Polymer Solar Cells. *J. Phys. Chem. C* **2013**, *117*, 14920−14928.
(72) Tremolet De Villers, B. J.; O'Hara, K. A.; Ostrowski, D. P.; Biddle, P. H.; Shaheen, S. E.; Chabinyc, M. L.; Olson, D. C.; Kopidakis, N. Removal of Residual Diiodooctane Improves Photostability of High-Performance Organic Solar Cell Polymers. *Chem. Mater.* **2016**, *28*, 876−884.
(73) Murgatroyd, P. N. Theory of Space-Charge-Limited Current Enhanced by Frenkel Effect. *J. Phys. D: Appl. Phys.* **1970**, *3*, 151−156.
(74) Blakesley, J. C.; Castro, F. A.; Kylberg, W.; Dibb, G. F. A.; Arantes, C.; Valaski, R.; Cremona, M.; Kim, J. S.; Kim, J.-S. Towards Reliable Charge-Mobility Benchmark Measurements for Organic Semiconductors. *Org. Electron.* **2014**, *15*, 1263−1272.
(75) Foster, S.; Deledalle, F.; Mitani, A.; Kimura, T.; Kim, K.-B.; Okachi, T.; Kirchartz, T.; Oguma, J.; Miyake, K.; Durrant, J. R.; et al. Electron Collection as a Limit to Polymer:PCBM Solar Cell Efficiency: Effect of Blend Microstructure on Carrier Mobility and Device Performance in PTB7:PCBM. *Adv. Energy Mater.* **2014**, *4*, 1400311.


DOI: 10.1021/acs.jpcc.8b02859
*J. Phys. Chem. C* 2018, 122, 15078−15089

(76) Manley, E. F.; Strzalka, J.; Fauvell, T. J.; Jackson, N. E.; Leonardi, M. J.; Eastham, N. D.; Marks, T. J.; Chen, L. X. In Situ GIWAXS Analysis of Solvent and Additive Effects on PTB7 Thin Film Microstructure Evolution During Spin Coating. *Adv. Mater.* **2017**, *29*, 1703933.
(77) Scholes, D. T.; Yee, P. Y.; Lindemuth, J. R.; Kang, H.; Onorato, J.; Ghosh, R.; Luscombe, C. K.; Spano, F. C.; Tolbert, S. H.; Schwartz, B. J. The Effects of Crystallinity on Charge Transport and the Structure of Sequentially Processed F4TCNQ-Doped Conjugated Polymer Films. *Adv. Funct. Mater.* **2017**, *27*, 1702654.
(78) Scholes, D. T.; Hawks, S. A.; Yee, P. Y.; Wu, H.; Lindemuth, J. R.; Tolbert, S. H.; Schwartz, B. J. Overcoming Film Quality Issues for Conjugated Polymers Doped with F4TCNQ by Solution Sequential Processing: Hall Effect, Structural, and Optical Measurements. *J. Phys. Chem. Lett.* **2015**, *6*, 4786−4793.
(79) Dong, B. X.; Huang, B.; Tan, A.; Green, P. F. Nanoscale Orientation Effects on Carrier Transport in a Low-Band-Gap Polymer. *J. Phys. Chem. C* **2014**, *118*, 17490−17498.



DOI: 10.1021/acs.jpcc.8b02859
*J. Phys. Chem. C* 2018, 122, 15078−15089